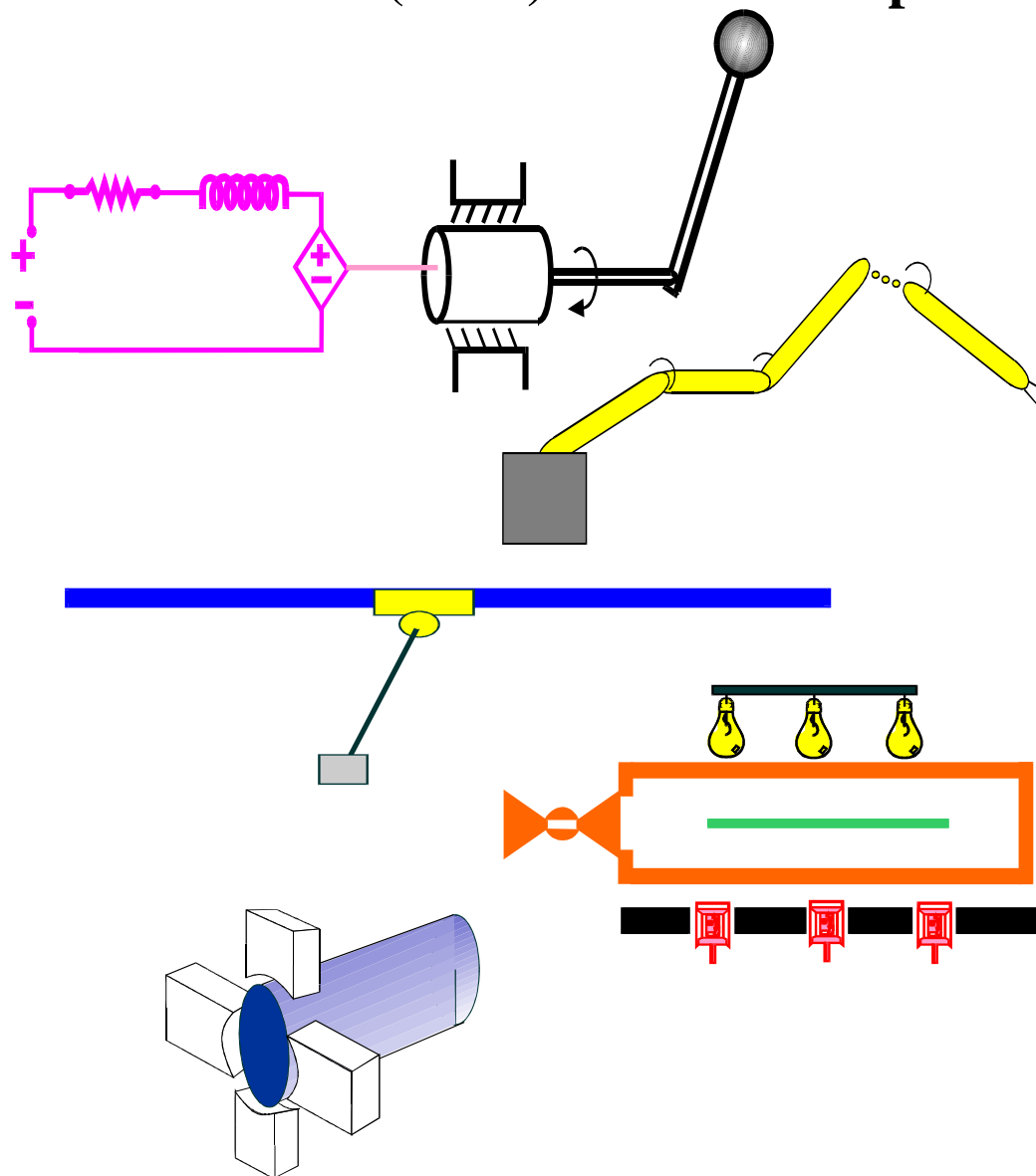


Clemson University
College of Engineering and Science
Control and Robotics (CRB) Technical Report



Number: CU/CRB/4/9/09/#1

Title: Nonlinear Robust Control to Maximize Energy Capture in a Variable Speed Wind Turbine Using an Induction Generator

Authors: Erhun Iyasere, Darren M. Dawson, John R. Wagner, Mohammed Salah and Enver Tatlicioglu

Nonlinear Robust Control to Maximize Energy Capture in a Variable Speed Wind Turbine Using an Induction Generator

Erhun Iyasere, Darren M. Dawson, John R. Wagner
College of Engineering and Science
Clemson University
Clemson, USA

Mohammed Salah
Department of Mechatronics Engineering
Hashemite University
Zarqa, Jordan

Enver Tatlicioglu
Department of Electrical and Electronics Engineering,
Izmir Institute of Technology
Urla, Turkey

Abstract—The emergence of wind turbine systems for electric power generation can help satisfy the growing global demand. This paper proposes a control strategy to maximize the wind energy captured in a variable speed wind turbine, with an internal induction generator, at low to medium wind speeds. The proposed strategy controls the tip speed ratio, via the rotor angular speed, to an optimum point at which the efficiency constant (or power coefficient) is maximal for a particular blade pitch angle and wind speed. This control method allows for aerodynamic rotor power maximization without exact wind turbine model knowledge. Representative numerical results demonstrate that the wind turbine can be controlled to achieve near maximum energy capture.

Key Words—*Induction generators, Lyapunov, robustness, torque control, wind power generation*

NOMENCLATURE

β	Blade pitch angle (rad).
C_p	Power capture efficiency.
I	Current (A).
L	Inductance (H).
λ	Tip speed ratio.
M	Mutual inductance (H).
M_m	Moment of inertia (kg.m ²).
n_p	Number of generator pole pairs.
ω	Rotor angular velocity (rad/s).
$\bar{\Psi}, \Psi$	Flux Linkage (Wb).
P	Power (W).
R	Resistance (Ω).

R_a	Blade radius.
ρ_a	Air density (kg/m ³).
τ_{em}	Electromagnetic torque (N.m).
v	Wind velocity (m/s ²)
V_r	Rotor Voltage (V)

Subscripts and Superscripts

*	Optimal value
a, b	Fixed stator frame component
d	Desired value
L	Load
max	Maximum value
r, s	Rotor, stator

I. INTRODUCTION

Wind energy has evolved into an attractive energy source for electric utilities, although it is currently responsible for about one percent of the global electrical power production. The structure of wind turbines, as well as the fact that the wind energy rate is uncontrollable, complicates the problem of regulating the power capture. This engineering challenge has been alleviated by the construction of variable speed wind turbines, which are designed to regulate the power captured over a range of operating speeds. However, the efficiency of power regulation is dependent on the selected control method.

The standard region 2 (power capture maximization mode) control scheme used for variable speed wind turbines, ($\tau = k\omega^2$, where τ is the control torque, ω is the rotor angular speed and k is a control gain), has some

disadvantages that can result in unsatisfactory power capture. First, the control gain k is difficult to determine due to the dependence on exact model knowledge (maximum power efficiency constant and optimal tip speed ratio). Secondly, the standard value of k might not provide the maximum energy capture under real world turbulent conditions. Johnson and Fingersh [1] showed via simulation that smaller values of k than the standard can result in increased power capture. They proposed a new control scheme: an adaptive control scheme that allows for maximum power capture in presence of parameter uncertainty. Similar adaptive control techniques for wind turbine control were developed in [2] and [3].

Other wind turbine control methods like classical control techniques [4]-[7], robust control [8] and fuzzy logic control [9]-[10] have been utilized to regulate rotor speed, regulate pitch angle and to enhance energy capture. Iyasere et al. [8] proposed a robust control strategy to control the blade pitch angle and rotor speed in a variable speed, variable pitch wind turbine in order to maximize the energy capture, without the knowledge of the optimal tip speed ratio and in the presence of model structural uncertainties.

An area of particular importance is the control of the internal generators used in wind turbines. The most commonly used generator is the induction generator; the types of which include cage, wound rotor and doubly fed induction generator (DFIG). The dynamic modeling [11]-[15] and control [16]-[23] of induction machines has been extensively researched. Thringer and Luomi [11] examined the validity of various dynamic models of induction machines to include the fifth-order Park model and other reduced order models by predicting the low frequency dynamic response of a 15 kW induction machine and comparing results to actual measurements. They concluded that the Park model accurately predicts rotor speed, electrical torque, active power, reactive power and stator current responses to perturbations in the shaft torque, supply frequency and voltage magnitude. In power system analysis, a third order model was determined to be the right fit of accuracy and simplicity. Tapia et al. [12] developed the mathematical model of a grid connected wind driven DFIG and presented a comparison of the simulation results to real machine performance results. They also developed a stator-flux-oriented vector control based technique to control the generator power factor. Mullane and O'Malley [13] examined the inertial response of a squirrel cage and a doubly fed induction wind turbine generator using fifth-order induction generator models. They discovered that a DFIG utilizing field-oriented control is strongly influenced by rotor current controller bandwidth. Hu and Dawson [16] presented an adaptive partial state feedback position tracking controller for the full-order nonlinear dynamic model for an induction motor. The controller compensates for uncertainty in rotor resistance and mechanical system parameters while yielding asymptotic rotor position tracking. Datta and Ranganathan [17] developed a simple position-sensorless strategy for rotor-side field-oriented control of a wound rotor induction machine. The algorithm is based on axis transformation with reduced dependence on machine parameters compared to

other methods. Pena et al. [18] describes a vector control scheme for the supply-side voltage source-converter of a DFIG for independent control of active and reactive power. This strategy was embedded into an optimal tracking controller in order to maximize energy capture in a wind energy application. Two tracking schemes were developed; speed mode and current mode.

In this study, a control strategy is developed to regulate the rotor speed of a small variable speed wind turbine system with an induction generator. The control objective is to maximize the energy captured by the wind turbine for low to medium air speeds by tracking a desired rotor speed in the presence of system nonlinearities and structural uncertainty. Additionally, the maximization of the energy captured is achieved without the knowledge of the relationship that governs the power capture efficiency of the wind turbine. Instead, an optimization algorithm is developed to seek the unknown optimal rotor speed that maximizes the energy captured (via the aerodynamic rotor power), at a particular blade pitch angle and wind speed, while ensuring that the resulting trajectory is sufficiently differentiable. The problem of not explicitly knowing the rotor speed *a priori* is countered by the fact that the optimal rotor speed will change as the wind speed changes which may be accommodated for by choosing the right optimization algorithm. A robust controller is designed and proven to yield a globally uniformly ultimately bounded (GUUB) stable closed loop system through Lyapunov-based analysis.

The paper is organized as follows. In Section II, the system model and problem statement are mathematically formulated. In Section III, a robust speed tracking controller is designed and the stability analysis is presented. In Section IV, an observer is designed to estimate the system nonlinearities. In Section V, the estimate of the system nonlinearities is used to generate the rotor speed reference trajectory followed by numerical simulation results in Section VI. Concluding remarks are presented in Section VII.

II. SYSTEM MODEL

The wind turbine model consists of a wind rotor, drive shaft and an internal induction generator. The system block diagram is shown in Fig. 1. The aerodynamic rotor power captured by the wind turbine is dependent on the available wind power and the power coefficient, C_p , which is a function of the tip-speed ratio (TSR) $\lambda(t) \in \mathbb{R}$, and the blade pitch angle, $\beta \in \mathbb{R}$. The rotor power of the wind turbine, $P_{\text{aero}}(t) \in \mathbb{R}$, can be defined as

$$P_{\text{aero}} = \frac{1}{2} C_p \rho_a \pi R_a^2 v^3 \quad (1)$$

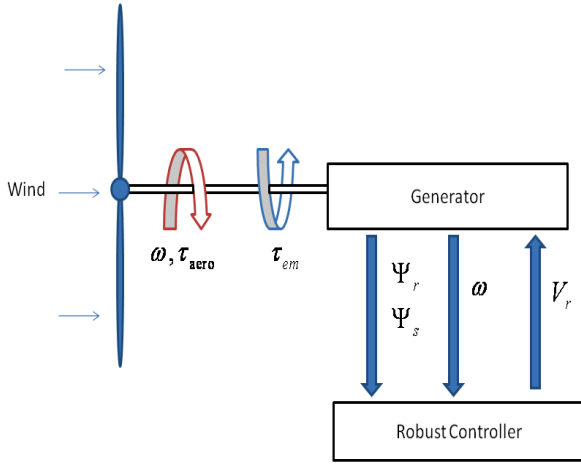


Figure 1. Block diagram of wind turbine system

where $C_p(\lambda, \beta) \in \mathbb{R}$ is assumed to be unknown. The tip-speed ratio, $\lambda(t)$, is defined as

$$\lambda = \frac{\omega R_a}{v}. \quad (2)$$

From (1) and (2), it can be inferred that there exists a constant optimal rotor speed, ω^* , for a particular wind speed, $v(t)$, and blade pitch angle, β , at which the power capture efficiency, and thus the aerodynamic rotor power is maximum,

$$\text{with } P_{\max} \triangleq \frac{1}{2} C_p^{\max} \rho_a \pi R_a^2 v^3,$$

$$C_p^{\max} = C_p(\lambda^*, \beta) \text{ and } \lambda^* = \frac{\omega^* R_a}{v} [1].$$

The rotor power, $P_{\text{aero}}(t)$, can also be written as

$$P_{\text{aero}} = \tau_{\text{aero}} \omega \quad (3)$$

where $\tau_{\text{aero}}(t) \in \mathbb{R}$ is the aerodynamic torque applied to the rotor by the wind. An expression for $\tau_{\text{aero}}(t)$ can be derived from (1)-(3) as

$$\tau_{\text{aero}} = \frac{1}{2} \rho_a \pi R_a^3 \frac{C_p}{\lambda} v^2. \quad (4)$$

Remark 1.1: In (1), it is assumed that $C_p(\cdot)$ is unknown which implies that $\tau_{\text{aero}}(t)$ and $P_{\text{aero}}(t)$ are unmeasurable.

A. Mechanical Subsystem Dynamics

The mechanical subsystem describes the rotor dynamics of the variable speed wind turbine and is assumed to be of the form

$$M_m \dot{\omega} + f = \tau_{em} \quad (5)$$

where $\dot{\omega}(t)$ is the rotor acceleration, and $f(\omega, v) \triangleq -\tau_{\text{aero}}(t)$ represents the system nonlinearities.

B. Electrical Subsystem Dynamics

The standard induction machine model can be found in [24]. The model utilized in this paper is the transformed nonlinear induction machine model in the stator fixed a - b reference frame with the assumptions of equal mutual and auto inductances, and a linear magnetic circuit [19]. The electrical dynamics of the internal induction generator can be described by the following dynamic equations:

$$\dot{\bar{\Psi}}_s = -(R_s + R_L) \bar{I}_s \quad (6)$$

$$\dot{\bar{\Psi}}_r = -R_r \bar{I}_r + n_p \omega J \bar{\Psi}_r + \bar{V}_r \quad (7)$$

$$\bar{I}_s = \kappa_1 \bar{\Psi}_s - \kappa_2 \bar{\Psi}_r \quad (8)$$

$$\bar{I}_r = \kappa_1 \bar{\Psi}_r - \kappa_2 \bar{\Psi}_s \quad (9)$$

$$\tau_{em} = \alpha \bar{\Psi}_s^T J \bar{\Psi}_r \quad (10)$$

$$J = \begin{bmatrix} 0 & -1 \\ 1 & 0 \end{bmatrix}, \quad \alpha = n_p \kappa_2 \quad (11)$$

where $\bar{\Psi}_s = [\bar{\Psi}_{s_a}, \bar{\Psi}_{s_b}]^T$, $\bar{\Psi}_r = [\bar{\Psi}_{r_a}, \bar{\Psi}_{r_b}]^T$, $\bar{V}_r = [\bar{V}_{r_a}, \bar{V}_{r_b}]^T$, $\bar{I}_s = [\bar{I}_{s_a}, \bar{I}_{s_b}]^T$, $\bar{I}_r = [\bar{I}_{r_a}, \bar{I}_{r_b}]^T \in \mathbb{R}^2$. In (8) and (9), κ_1 and κ_2 are constants related to the motor parameters, and are given explicitly by

$$\kappa_1 = \frac{L_s}{L_s^2 - M^2}, \quad \kappa_2 = \frac{M}{L_s^2 - M^2} \quad (12)$$

To facilitate control development, the following model characteristics are assumed:

Assumption 1: The parameters L_s , M , M_m , n_p , R , R_L , R_r , R_s , β and ρ_a are known constants.

Assumption 2: $\omega(t)$, $\bar{I}_s(t)$, $\bar{I}_r(t)$, and $v(t)$ are measurable.

Assumption 3: $v(t)$ is constant or slowly time varying (*i.e.*, $\dot{v} \cong 0$).

Assumption 4: $v(t)$, $\dot{v}(t)$, $\ddot{v}(t)$ are bounded.

Assumption 5: As a consequence of the fact that $\tau_{\text{aero}}(t)$ is unknown, $f(\omega, v)$, introduced in (5) is also unknown.

Assumption 6: The variables, $f(\cdot)$, $\dot{f}(\cdot)$, $\ddot{f}(\cdot)$ are bounded provided that $\omega(t)$, $\dot{\omega}(t)$, $\ddot{\omega}(t)$ are bounded.

Remark 2.1: $f(\omega, v)$ can be upper bounded by a known function such that $|f(\omega, v)| \leq \rho(\omega)$ where $\rho(\omega)$ is continuously differentiable for all $\omega(t) > 0$.

C. Electrical Subsystem Transformation

An auxiliary control input $\omega_s(t)$ is injected into the electrical subsystem dynamics via time-varying coordinate transformation [20] as follows

$$\begin{aligned} \Psi_s &\triangleq T\bar{\Psi}_s, & I_s &\triangleq T\bar{I}_s, & V_r &\triangleq T\bar{V}_r \\ \Psi_r &\triangleq T\Psi_r, & I_r &\triangleq T\bar{I}_r \end{aligned} \quad (13)$$

where $T(t) \in \mathbb{R}^{2 \times 2}$ is defined as

$$T \triangleq \begin{bmatrix} \cos(\varepsilon_0) & \sin(\varepsilon_0) \\ -\sin(\varepsilon_0) & \cos(\varepsilon_0) \end{bmatrix} \quad (14)$$

where $\dot{\varepsilon}_0 = \omega_s$. It should be noted that $T(t)$ satisfies $T^{-T}JT^{-1} = J$.

The overall dynamics of the induction generator can then be given by the following fifth order model:

$$M_m \dot{\omega} + f = \tau_{em} \quad (15)$$

$$\dot{\Psi}_s = -R_o \kappa_1 \Psi_s + R_o \kappa_2 \Psi_r - J \Psi_s \omega_s \quad (16)$$

$$\dot{\Psi}_r = V_r - R_r \kappa_1 \Psi_r + R_r \kappa_2 \Psi_s + n_p \omega J \Psi_r - J \Psi_r \omega_s \quad (17)$$

$$\tau_{em} = \alpha \Psi_s^T J \Psi_r \quad (18)$$

$$I_s = \kappa_1 \Psi_s - \kappa_2 \Psi_r \quad (19)$$

$$I_r = \kappa_1 \Psi_r - \kappa_2 \Psi_s \quad (20)$$

where $\Psi_s = [\Psi_{s_1}, \Psi_{s_2}]^T$, $\Psi_r = [\Psi_{r_1}, \Psi_{r_2}]^T$, $V_r = [V_{r_1}, V_{r_2}]^T$, $R_o \triangleq R_s + R_L$.

III. CONTROLLER DESIGN

A. Control Objective

The objective in this paper is to maximize the aerodynamic rotor power of the wind turbine, $P_{aero}(t)$, by tracking a developed desired rotor speed $\omega_d(t) \in \mathbb{R}$ such that $\omega(t) \rightarrow \omega_d(t)$ as $t \rightarrow \infty$. This is achieved in turn by tracking a desired electromagnetic torque, $\tau_d(t) \in \mathbb{R}$, a

desired stator flux $\Psi_s^d(t) \in \mathbb{R}^{2 \times 1}$, and a desired rotor flux $\Psi_r^d(t) \in \mathbb{R}^{2 \times 1}$ such that $\Psi_s(t) \rightarrow \Psi_s^d(t)$, $\Psi_r(t) \rightarrow \Psi_r^d(t)$, and $\tau_{em}(t) \rightarrow \tau_d(t)$ as $t \rightarrow \infty$ where

$$\Psi_s^d = [\Psi_{s_1}^d, 0]^T \quad \Psi_r^d = [\Psi_{r_1}^d, \Psi_{r_2}^d]^T \quad (21)$$

$$\tau_d \triangleq \alpha (\Psi_s^d)^T J \Psi_r^d \quad (22)$$

Remark 3.1: The desired rotor speed, $\omega_d(t)$, is designed online using a numerical-based optimization algorithm, as shown in Section V, to maximize the rotor power $P_{aero}(t)$ at a particular blade pitch angle, β , and wind velocity, $v(t)$, such that $\omega_d(t) \rightarrow \omega^*$, where the optimal speed, ω^* , is the result of the optimum seeking algorithm after convergence, hence $P_{aero}(t) \rightarrow P_{max}$ if $\omega(t) \rightarrow \omega_d(t)$. Additionally, $\omega_d(t)$ is designed such that $\omega_d(t), \dot{\omega}_d(t), \ddot{\omega}_d(t) \in \mathcal{L}_\infty$.

Remark 3.2: The desired rotor flux, $\Psi_{s_1}^d(t)$, is designed such that $\Psi_{s_1}^d(t) > 0$, $\Psi_{s_1}^d(t), \dot{\Psi}_{s_1}^d(t), \ddot{\Psi}_{s_1}^d(t) \in \mathcal{L}_\infty$, and power loss in the system is minimized, as shown in Appendix I.

Remark 3.3: To ensure equality in (22), $\Psi_{r_2}^d(t)$ is designed such that $\Psi_{r_2}^d = \frac{-\tau_d}{\alpha \Psi_{s_1}^d}$.

B. Error System Development

To quantify the stated control objective, rotor speed, stator flux and rotor flux tracking errors denoted by $e(t) \in \mathbb{R}$, $\eta_s(t), \eta_r(t) \in \mathbb{R}^{2 \times 1}$ respectively, are defined as

$$e \triangleq \omega_d - \omega \quad (23)$$

$$\eta_s = \begin{bmatrix} \eta_{s_1} \\ \eta_{s_2} \end{bmatrix} = \begin{bmatrix} \Psi_{s_1}^d \\ 0 \end{bmatrix} - \begin{bmatrix} \Psi_{s_1} \\ \Psi_{s_2} \end{bmatrix} \quad (24)$$

$$\eta_r = \begin{bmatrix} \eta_{r_1} \\ \eta_{r_2} \end{bmatrix} = \begin{bmatrix} \Psi_{r_1}^d \\ \Psi_{r_2}^d \end{bmatrix} - \begin{bmatrix} \Psi_{r_1} \\ \Psi_{r_2} \end{bmatrix} \quad (25)$$

where $\eta_{s_1}(t), \eta_{s_2}(t), \eta_{r_1}(t), \eta_{r_2}(t) \in \mathbb{R}$.

From the definition of the tracking errors in (23), and subsystem dynamics in (5), a rotor speed open loop error system is developed as follows

$$M_m \dot{e} = M_m \dot{\omega}_d + f - \tau_{em} \quad (26)$$

Substituting in (18) and adding and subtracting (22) to the right hand side of (26) results in

$$M_m \dot{e} = M_m \dot{\omega}_d + f - \tau_d + \alpha \left[\begin{pmatrix} \Psi_s^d \\ \Psi_r^d \end{pmatrix}^T J \Psi_r^d - \Psi_s^T J \Psi_r \right]. \quad (27)$$

Substituting in (24) and (25) into (27), and performing simple algebraic manipulations, results in

$$M_m \dot{e} = M_m \dot{\omega}_d + f - \tau_d - \alpha \Psi_{s_1}^d \eta_{r_2} + \alpha \Psi_{r_1}^d \eta_{s_2} - \alpha \Psi_{r_2}^d \eta_{s_1} - \alpha \eta_{s_2} \eta_{r_1} + \alpha \eta_{s_1} \eta_{r_2}. \quad (28)$$

Similarly, the stator and rotor flux open loop error systems are developed as follows

$$\begin{bmatrix} \dot{\eta}_{s_1} \\ \dot{\eta}_{s_2} \end{bmatrix} = \begin{bmatrix} \dot{\Psi}_{s_1}^d \\ 0 \end{bmatrix} + R_o \kappa_1 \begin{bmatrix} \Psi_{s_1}^d \\ 0 \end{bmatrix} - R_o \kappa_1 \begin{bmatrix} \eta_{s_1} \\ \eta_{s_2} \end{bmatrix} + R_o \kappa_2 \begin{bmatrix} \eta_{r_1} \\ \eta_{r_2} \end{bmatrix} - R_o \kappa_2 \begin{bmatrix} \Psi_{r_1}^d \\ \Psi_{r_2}^d \end{bmatrix} + \begin{bmatrix} 0 \\ \Psi_{s_1}^d \end{bmatrix} \omega_s + \begin{bmatrix} \eta_{s_2} \\ -\eta_{s_1} \end{bmatrix} \omega_s \quad (29)$$

$$\begin{bmatrix} \dot{\eta}_{r_1} \\ \dot{\eta}_{r_2} \end{bmatrix} = \begin{bmatrix} \dot{\Psi}_{r_1}^d \\ \dot{\Psi}_{r_2}^d \end{bmatrix} + R_r \kappa_2 \begin{bmatrix} \eta_{s_1} \\ \eta_{s_2} \end{bmatrix} - R_r \kappa_2 \begin{bmatrix} \Psi_{s_1}^d \\ 0 \end{bmatrix} + R_r \kappa_1 \begin{bmatrix} \Psi_{r_1}^d \\ \Psi_{r_2}^d \end{bmatrix} - R_r \kappa_1 \begin{bmatrix} \eta_{r_1} \\ \eta_{r_2} \end{bmatrix} + n_p \omega \begin{bmatrix} -\eta_{r_2} \\ \eta_{r_1} \end{bmatrix} - n_p \omega \begin{bmatrix} -\Psi_{r_2}^d \\ \Psi_{r_1}^d \end{bmatrix} - \begin{bmatrix} V_{r_1} \\ V_{r_2} \end{bmatrix} + \begin{bmatrix} -\Psi_{r_2}^d \\ \Psi_{r_1}^d \end{bmatrix} \omega_s - \begin{bmatrix} -\eta_{r_2} \\ \eta_{r_1} \end{bmatrix} \omega_s \quad (30)$$

where (16), (17), and the time derivatives of (24) and (25) were utilized.

C. Control Input Design

The control inputs will be designed based on the subsequent stability analysis as well as the structure of the open loop error systems in (28)-(30).

The desired torque trajectory, $\tau_d(t)$ is designed to be

$$\tau_d = Ke + \frac{\rho^2(\omega)e}{\varepsilon} + M_m \dot{\omega}_d - \hat{f}_s \quad (31)$$

where $\hat{f}_s(\cdot) \triangleq \frac{1}{\sigma_s + 1} \text{sat}\{\hat{f}(\cdot)\}$, $\text{sat}\{\cdot\}$ is the saturation function, $\hat{f}(\cdot)$ is an estimate of $f(\cdot)$ designed later in Section IV, $s \in \mathbb{C}$ is the Laplace variable, $K \in \mathbb{R}^+$ is a control gain, $\varepsilon, \sigma \in \mathbb{R}^+$ are constants and $\rho(\omega)$ was previously defined in Remark 2.1.

Remark 3.4: Since $\frac{1}{\sigma_s + 1}$ is a proper bounded filter and the output of the saturation function is always bounded then it can be concluded that $\hat{f}_s(\cdot), \hat{f}_s(\cdot) \in \mathcal{L}_\infty$. Thus, it may be concluded that $|\hat{f}_s(\cdot)| \leq \rho_s$ where $\rho_s \in \mathbb{R}^+$.

The first entry of the desired rotor flux, $\Psi_{r_1}^d(t)$, is designed to be

$$\Psi_{r_1}^d = \frac{1}{R_o \kappa_2} \left[\dot{\Psi}_{s_1}^d + R_o \kappa_1 \Psi_{s_1}^d - \alpha \Psi_{r_2}^d e - R_o \kappa_1 \eta_{s_1} + \kappa_{s_1} \eta_{s_1} \right] \quad (32)$$

where $\kappa_{s_1} \in \mathbb{R}^+$ is a control gain. The auxiliary control input, $\omega_s(t)$, is designed to be

$$\omega_s = \frac{1}{\Psi_{s_1}^d} \left[R_o \kappa_2 \Psi_{r_2}^d - \alpha \Psi_{r_1}^d e + R_o \kappa_1 \eta_{s_2} - \kappa_{s_2} \eta_{s_2} \right] \quad (33)$$

where $\kappa_{s_2} \in \mathbb{R}^+$ is a control gain.

The control voltage, $V_r(t)$ is designed as follows

$$V_{r_1} = \frac{\ddot{\Psi}_{s_1}^d}{R_o \kappa_2} + \Theta_1 \dot{\Psi}_{s_1}^d - \Theta_2 \Psi_{s_1}^d + \Theta_3 \Psi_{r_1}^d + \Theta_4 \Psi_{r_2}^d + (\Theta_5 - \Theta_6 e + \Theta_7 e^2) e + (\Theta_8 - \Theta_9 \Psi_{r_2}^d e) \eta_{s_1} - (\Theta_{10} + \Theta_{11} e) \eta_{s_2} + (\Theta_{12} - \Theta_9 e) \eta_{s_2} \eta_{r_1} + \Theta_{13} \eta_{r_1} \quad (34)$$

$$V_{r_2} = \Omega_1 - \Omega_2 \hat{f}_s - \Omega_3 e + \alpha e \eta_{s_1} + \Omega_4 \Psi_{r_2}^d \eta_{s_1} + \Omega_5 \eta_{s_2} + \frac{\alpha^2 \Psi_{s_1}^d \Psi_{r_2}^d}{R_o \kappa_2 M_m} \eta_{r_1} - (\Omega_6 - \Omega_7 \eta_{s_1}) e \eta_{r_1} - \frac{\alpha^2 \Psi_{r_2}^d}{R_o \kappa_2 M_m} \eta_{s_1} \eta_{r_1} + \Omega_8 \eta_{s_2} \eta_{r_1} - \Omega_8 \eta_{s_1} \eta_{r_2} + \Omega_9 \eta_{r_2} - \Omega_{10} e^2 \quad (35)$$

where the terms $\Theta_i(t), \Omega_j(t)$, $i=1, \dots, 13$ and $j=1, \dots, 10$, are explicitly defined in Appendix II.

D. Analysis of tracking error systems

Theorem 1: Given the error system in (28)-(30) and the designed terms in (31)-(35), all signals are bounded and the tracking error signals given in (23)-(25) are globally uniformly ultimately bounded (GUUB).

Proof: A non-negative function, denoted by $V(t) \in \mathbb{R}$, is defined as

$$V = 0.5 M_m e^2 + 0.5 \eta_s^T \eta_s + 0.5 \eta_r^T \eta_r. \quad (36)$$

The Lyapunov function $V(t)$ can be written as

$$V = 0.5z^T \text{diag}\{M_m, 1, 1, 1, 1\}z \quad (37)$$

and can thus be bounded using the Raleigh inequality as

$$\lambda_{\min} \|z\|^2 \leq V \leq \lambda_{\max} \|z\|^2 \quad (38)$$

where $z(t) \in \mathbb{R}^5$ is defined as $z = \begin{bmatrix} e & \eta_s^T & \eta_r^T \end{bmatrix}^T$, $\lambda_{\min} = 0.5 \min(M_m, 1)$ and $\lambda_{\max} = 0.5 \max(M_m, 1)$.

Taking the time derivative of (36) results in

$$\dot{V} = eM_m \dot{e} + \begin{bmatrix} \eta_{s_1} & \eta_{s_2} \end{bmatrix} \begin{bmatrix} \dot{\eta}_{s_1} \\ \dot{\eta}_{s_2} \end{bmatrix} + \begin{bmatrix} \eta_{r_1} & \eta_{r_2} \end{bmatrix} \begin{bmatrix} \dot{\eta}_{r_1} \\ \dot{\eta}_{r_2} \end{bmatrix}. \quad (39)$$

After substituting (28)-(30) into (39), $\dot{V}(t)$ can be expressed as

$$\begin{aligned} \dot{V} = & e \left[M_m \dot{\omega}_d + f - \tau_d - \alpha \Psi_{s_1}^d \eta_{r_2} + \alpha \Psi_{r_1}^d \eta_{s_2} \right. \\ & \left. - \alpha \Psi_{r_2}^d \eta_{s_1} - \alpha \eta_{s_2} \eta_{r_1} + \alpha \eta_{s_1} \eta_{r_2} \right] + \begin{bmatrix} \eta_{s_1} \\ \eta_{s_2} \end{bmatrix}^T \left\{ \begin{bmatrix} \Psi_{s_1}^d \\ 0 \end{bmatrix} \right. \\ & \left. + R_o \kappa_1 \begin{bmatrix} \Psi_{s_1}^d \\ 0 \end{bmatrix} - R_o \kappa_1 \begin{bmatrix} \eta_{s_1} \\ \eta_{s_2} \end{bmatrix} + R_o \kappa_2 \begin{bmatrix} \eta_{r_1} \\ \eta_{r_2} \end{bmatrix} \right\} \\ & - R_o \kappa_2 \begin{bmatrix} \Psi_{r_1}^d \\ \Psi_{r_2}^d \end{bmatrix} + \begin{bmatrix} 0 \\ \Psi_{s_1}^d \end{bmatrix} \omega_s + \begin{bmatrix} \eta_{s_2} \\ -\eta_{s_1} \end{bmatrix} \omega_s \quad (40) \\ & + (\eta_{r_1} \quad \eta_{r_2}) \left\{ \begin{bmatrix} \dot{\Psi}_{r_1}^d \\ \dot{\Psi}_{r_2}^d \end{bmatrix} + R_r \kappa_2 \begin{bmatrix} \eta_{s_1} \\ \eta_{s_2} \end{bmatrix} - R_r \kappa_2 \begin{bmatrix} \Psi_{s_1}^d \\ 0 \end{bmatrix} \right. \\ & \left. + R_r \kappa_1 \left(\begin{bmatrix} \Psi_{r_1}^d \\ \Psi_{r_2}^d \end{bmatrix} - \begin{bmatrix} \eta_{r_1} \\ \eta_{r_2} \end{bmatrix} \right) - \begin{bmatrix} V_{r_1} \\ V_{r_2} \end{bmatrix} + \begin{bmatrix} -\Psi_{r_2}^d \\ \Psi_{r_1}^d \end{bmatrix} \omega_s \right\} \end{aligned}$$

Substituting (31)-(35) as well as the mathematical derivatives of $\Psi_{r_1}^d(t)$ and $\Psi_{r_2}^d(t)$, results in

$$\begin{aligned} \dot{V} = & ef + e\hat{f}_s - Ke^2 - \kappa_{s_1} \eta_{s_1}^2 - \kappa_{s_2} \eta_{s_2}^2 - \kappa_{r_1} \eta_{r_1}^2 - \kappa_{r_2} \eta_{r_2}^2 \\ & - \frac{\rho^2(\omega)e^2}{\varepsilon} - \frac{\rho_1^2(\cdot)\eta_{r_1}^2}{\varepsilon_1} - \frac{\rho_2^2(\cdot)\eta_{r_2}^2}{\varepsilon_2} \\ & + \frac{\left(\begin{array}{c} (2Ke + M_m \dot{\omega}_d + \hat{f}_s) \\ 2\rho(\omega)e(\partial\rho(\omega)e - \rho(\omega)) \end{array} \right)}{\varepsilon} f(\cdot)\eta_{r_1} \\ & - \left(K - \frac{\rho(\omega)(2\partial\rho(\omega)e - \rho(\omega))}{\varepsilon} \right) \frac{f(\cdot)\eta_{r_2}}{\alpha M_m \Psi_{s_1}^d} \quad (41) \end{aligned}$$

where $\partial\rho(\omega)$ denotes the partial derivative of $\rho(\omega)$ with respect to ω .

Remark 3.5: The functions $\rho_1(\cdot)$ and $\rho_2(\cdot)$ are designed in Appendix III such that

$$\rho_1(\cdot) \geq \frac{\left| \left(\begin{array}{c} 2Ke + M_m \dot{\omega}_d + \hat{f}_s \\ 2\rho(\omega)e(\partial\rho(\omega)e - \rho(\omega)) \end{array} \right) f \right|}{\left| R_o \kappa_2 M_m \Psi_{s_1}^d \right|} \quad (42)$$

$$\rho_2(\cdot) \geq \left| \left(K - \frac{2\rho(\omega)\partial\rho(\omega)}{\varepsilon} + \frac{\rho^2(\omega)}{\varepsilon} \right) \frac{f}{\alpha M_m \Psi_{s_1}^d} \right| \quad (43)$$

From (41), using Remarks 2.1, 3.4 and 3.5, the function $\dot{V}(t)$ can be upper bounded as follows

$$\begin{aligned} \dot{V} \leq & -K_1 e^2 - \kappa_{s_1} \eta_{s_1}^2 - \kappa_{s_2} \eta_{s_2}^2 - \kappa_{r_1} \eta_{r_1}^2 - \kappa_{r_2} \eta_{r_2}^2 \\ & + \{\rho_s |e| - K_2 e^2\} + \rho(\cdot) |e| \left[1 - \frac{\rho(\cdot)|e|}{\varepsilon} \right] \\ & + \rho_1(\cdot) |\eta_{r_1}| \left[1 - \frac{\rho_1(\cdot)|\eta_{r_1}|}{\varepsilon_1} \right] \\ & + \rho_2(\cdot) |\eta_{r_2}| \left[1 - \frac{\rho_2(\cdot)|\eta_{r_2}|}{\varepsilon_2} \right]. \quad (44) \end{aligned}$$

where the control gain, K , introduced in (31) is designed as $K = K_1 + K_2$ with $K_1, K_2 \in \mathbb{R}^+$. Applying the nonlinear damping argument [25] to the terms in the curly bracket on the right hand side of (44) results in the following upper bound for $\dot{V}(t)$

$$\dot{V} \leq -\gamma \|z\|^2 + \bar{\varepsilon} \quad (45)$$

where $\bar{\varepsilon}, \gamma \in \mathbb{R}^+$ and are defined as $\bar{\varepsilon} = \varepsilon + \varepsilon_1 + \varepsilon_2 + \frac{\rho_s^2}{K_2}$

and $\gamma = \min(K_1, \kappa_{s_1}, \kappa_{s_2}, \kappa_{r_1}, \kappa_{r_2})$.

From (38) and (45), the following relationship is obtained.

$$\dot{V} \leq -\frac{\gamma V}{\lambda_{\max}} + \bar{\varepsilon} \quad (46)$$

From (38) and (46), the error signal $\|z(t)\|$ can be upper bounded as

$$\|z(t)\| \leq \sqrt{\beta_0 \exp(-\beta_1 t) + \beta_2 [1 - \exp(-\beta_1 t)]} \quad (47)$$

where $\beta_0 \triangleq \frac{\lambda_{\max} \|z(t_0)\|^2}{\lambda_{\min}}$, $\beta_1 \triangleq \frac{\gamma}{\lambda_{\max}}$, and $\beta_2 \triangleq \frac{\lambda_{\max} \bar{\mathcal{E}}}{\lambda_{\min} \gamma}$.

From (47), it can be shown that $e(t), \eta_s(t), \eta_r(t) \in \mathcal{L}_\infty$. Since $e(t) \in \mathcal{L}_\infty$, (23) can be used along with Remark 3.1, to show that $\omega(t) \in \mathcal{L}_\infty$. After utilizing the fact that $\omega(t) \in \mathcal{L}_\infty$, from Assumption 6, it is apparent that $f(\cdot) \in \mathcal{L}_\infty$. After using Remarks 3.1 and 3.4 and the fact that $e(t) \in \mathcal{L}_\infty$, along with (31), it can be shown that $\tau_d(t) \in \mathcal{L}_\infty$. Remark 3.3 can be used along with the facts that $\tau_d(t), \Psi_{s_1}^d(t) \in \mathcal{L}_\infty$ to show that $\Psi_{r_2}^d(t) \in \mathcal{L}_\infty$. The expression in (32) can be used along with the above boundedness statements to show that $\Psi_{r_1}^d(t) \in \mathcal{L}_\infty$. Since all the signals on the right-hand-side of (28) are bounded then it can be concluded that $\dot{e}(t)$ is also bounded. From the time derivative of (23), it is easy to see that $\dot{\omega}(t)$ is bounded; thus from Assumption 6, it is clear that $\dot{f}(\cdot)$ is bounded. The mechanical subsystem dynamics in (5) can be utilized to show that $\tau_{em}(t)$ is bounded. Above boundedness statements can be utilized along with (24), (25) and (33) to show that $\Psi_s(t), \Psi_r(t), \omega_s(t) \in \mathcal{L}_\infty$. Since $\omega(t)$ and $\dot{\omega}(t)$ are bounded, it is clear that $\dot{\rho}(\cdot) \in \mathcal{L}_\infty$. Above boundedness statements can be used along with Assumption 4, Remarks 3.1, 3.2 and 3.4 to prove that all the terms in Appendices III and IV are bounded; thus from (34) and (35), it can be concluded that $V_{r_1}(t), V_{r_2}(t) \in \mathcal{L}_\infty$. After utilizing the fact that $\dot{\Psi}_{s_1}^d(t) \in \mathcal{L}_\infty$ along with the above boundedness statements, from (29), it is easy to see that $\dot{\eta}_s(t) \in \mathcal{L}_\infty$. The time derivatives of (31) and (32) can be utilized to show that $\dot{\tau}_d(t)$ and $\dot{\Psi}_{r_1}^d(t)$ are bounded. $\dot{\Psi}_{r_2}^d(t)$ can be shown to be bounded from the time derivative of the expression in Remark 3.3. From (30), it can be concluded that $\dot{\eta}_{r_1}(t), \dot{\eta}_{r_2}(t) \in \mathcal{L}_\infty$. The fact that $\dot{\eta}_s(t), \dot{\eta}_r(t) \in \mathcal{L}_\infty$ can be used along with the time derivatives of (24) and (25) to show that $\dot{\Psi}_s(t)$ and $\dot{\Psi}_r(t)$ are bounded; thus from the time derivative of (18), it is clear that $\dot{\tau}_{em}(t)$ is bounded. After taking the time derivative of (5), it can be concluded that $\dot{\omega}(t) \in \mathcal{L}_\infty$; thus from the second time derivative of (23), it is clear that $\ddot{e}(t) \in \mathcal{L}_\infty$ where Remark 3.1 is utilized. From Assumption 6, it may be concluded that $\ddot{f}(\cdot) \in \mathcal{L}_\infty$. The application of standard signal chasing arguments permits the conclusion that all signals in the closed loop system remain bounded.

IV. NONLINEARITY OBSERVER DESIGN

The control objective is to maximize the aerodynamic rotor power captured by a variable speed wind turbine with

structurally uncertain system nonlinearities by controlling the rotor speed, $\omega(t)$. The existence of uncertain system nonlinearities motivates the design of a system nonlinearity observer, denoted by $\hat{f}(\cdot) \in \mathbb{R}$, to estimate $f(\cdot)$. This estimate is developed for two reasons:

- $\hat{f}(\cdot)$ is used as a feed-forward term in the control design through $\hat{f}_s(\cdot)$.
- Since $P_{\text{aero}}(t)$ is unmeasurable, an estimate of the captured power, denoted by $\hat{P}_{\text{aero}}(t) \in \mathbb{R}$, is designed where $\hat{P}_{\text{aero}}(t) = -\hat{f}(t)\omega(t)$, and is used in the online planning of $\omega_d(t)$.

A. Observation Error Systems

The main objective of the observer is to observe the system nonlinearities $f(\cdot)$ such that $\hat{f}(\cdot) \rightarrow f(\cdot)$ as $t \rightarrow \infty$. To facilitate the observer design, the following system model is developed

$$M_m \dot{\hat{\omega}} = \tau_{em} - \hat{f} \quad (48)$$

where $\hat{\omega}(t) \in \mathbb{R}$ denotes the estimated rotor speed.

The rotor speed and nonlinearity observation errors, $\tilde{\omega}(t), \tilde{f}(t) \in \mathbb{R}$ are defined as

$$\tilde{\omega} \triangleq \hat{\omega} - \omega, \quad \tilde{f} \triangleq \hat{f} - f. \quad (49)$$

In addition, the filtered rotor speed observation error, denoted by $r(t) \in \mathbb{R}$, is defined to facilitate the subsequent design and analysis as

$$r \triangleq \dot{\tilde{\omega}} + k \tilde{\omega} \quad (50)$$

where $k \in \mathbb{R}^+$ is a control gain. After taking the time derivative of (50) and pre-multiplying by M_m , it can be seen that

$$M_m \dot{r} = -\dot{\tilde{f}} + \dot{f} + \Phi - \tilde{\omega} \quad (51)$$

where $\Phi(t) \in \mathbb{R}$ is defined as $\Phi = kM_m \dot{\tilde{\omega}} + \tilde{\omega}$.

Remark 4.1: The mean value theorem can be utilized to upper bound $\Phi(t)$ such that $|\Phi(t)| \leq \rho_N \|X\|$ where $X(t) = [\tilde{\omega}(t), r(t)]^T \in \mathbb{R}^2$ and $\rho_N \in \mathbb{R}^+$ is a bounding constant [26].

B. Observer Design

Based on the structure of (51), as well as the subsequent stability analysis, a continuous estimator law is proposed to achieve the stated estimator objectives with

$$\dot{\hat{f}} = (k_f + k)r + \rho_0 \operatorname{sgn}(\tilde{\omega}) \quad (52)$$

where $k_f, \rho_0 \in \mathbb{R}^+$ are control gains and $\operatorname{sgn}(\cdot) \in \mathbb{R}$ is the standard signum function.

C. Analysis of observer error systems

Before presenting the stability analysis, the following lemma will be introduced and later invoked.

Lemma: Let the auxiliary function $L(t) \in \mathbb{R}$ be defined as

$$L \triangleq r(\dot{f} - \rho_0 \operatorname{sgn}(\tilde{\omega})) \quad (53)$$

If the control gain ρ_0 is selected to satisfy the sufficient condition $\rho_0 > |\dot{f}(\cdot)| + \frac{|\ddot{f}(\cdot)|}{k}$, then $\int_{t_0}^t L(v)dv \leq \zeta$ where $\zeta \in \mathbb{R}^+$ is defined as

$$\zeta \triangleq \rho_0 |\tilde{\omega}(t_0)| - \tilde{\omega}(t_0) \dot{f}(t_0) \quad (54)$$

Proof: See Appendix IV.

Theorem 2: The observer design in (52) ensures that all system signals are bounded and asymptotic tracking in the sense that $\tilde{\omega}(t), \dot{\tilde{\omega}}(t), r(t) \rightarrow 0$ and $\hat{f}(t) \rightarrow f(t)$ as $t \rightarrow \infty$.

Proof: Define an auxiliary function $P(t) \in \mathbb{R}$ as

$$P = \zeta - \int_{t_0}^t L(v)dv \quad (55)$$

where $\zeta, L(t)$ have been defined in Lemma 1. Based on the non-negativity of $P(t)$ (see proof of Lemma), we define a nonnegative function $V_o(t) \in \mathbb{R}$ as follows

$$V_o(t) = \frac{1}{2} \tilde{\omega}^2 + \frac{1}{2} M_m r^2 + P \quad (56)$$

After taking the time derivative of (56) and utilizing (51), (53), and the time derivative of (55), we can conveniently rearrange terms to obtain the following expression

$$\dot{V}_o = -k\tilde{\omega}^2 - r\dot{f} + r\Phi + r\rho_0 \operatorname{sgn}(\tilde{\omega}) \quad (57)$$

After substituting (52) and utilizing Remark 4.1, simple algebraic manipulations can be used to obtain the following upper bound for $\dot{V}_o(t)$

$$\dot{V}_o \leq -k\|X\|^2 + \left[|r|\rho_N \|X\| - k_f |r|^2 \right] \quad (58)$$

Applying the nonlinear damping argument [25] to the bracketed term in (58) results in the following upper bound for $\dot{V}_o(t)$

$$\dot{V}_o \leq -\left[k - \frac{\rho_N^2}{k_f} \right] \|X\|^2 \quad (59)$$

From (59), it is possible to state that

$$\dot{V}_o \leq -\zeta \|X\|^2 \quad \text{for } k_f > \frac{\rho_N^2}{k} \quad (60)$$

where $\zeta \in \mathbb{R}^+$ is a constant. From (60) and the analysis in this section, we can conclude that $X(t) \in \mathcal{L}_\infty$. From the definition of $X(t)$, it can be inferred that

$\tilde{\omega}(t), \dot{\tilde{\omega}}(t), r(t) \in \mathcal{L}_\infty$. From (52), it is clear that $\dot{f}(\cdot) \in \mathcal{L}_\infty$. Using standard signal chasing arguments, it can be shown that the all the signals in the closed-loop system remain bounded. In particular, from (51), it can be seen that $\dot{r}(t) \in \mathcal{L}_\infty$; thus $\dot{X}(t) \in \mathcal{L}_\infty$. After employing a corollary to Barbalat's Lemma [26], it is easy to show that $\|X(t)\| \rightarrow 0$ as $t \rightarrow \infty$. From the definition of $X(t)$, it can be concluded that $\tilde{\omega}(t), r(t) \rightarrow 0$ as $t \rightarrow \infty$. From (50), it is easy to see that $\dot{\tilde{\omega}}(t) \rightarrow 0$ as $t \rightarrow \infty$.

From (48), the following relationship can be obtained

$$M_m \dot{\tilde{\omega}} = f - \hat{f} = -\tilde{f} \quad (61)$$

From (61), it is clear that $\dot{\tilde{\omega}}(t) \rightarrow 0$ implies that $|\tilde{f}(t)| \rightarrow 0$ thus $\hat{f}(t) \rightarrow f(t)$ so $\hat{P}_{\text{aero}}(t) \rightarrow P_{\text{aero}}(t)$ as $t \rightarrow \infty$.

V. TRAJECTORY GENERATOR

In Remark 3.1, it is assumed that a desired trajectory $\omega_d(t)$ can be designed such that $\omega_d(t), \dot{\omega}_d(t)$ and $\ddot{\omega}_d(t)$ are bounded and $\omega_d(t) \rightarrow \omega^*$, where ω^* is the unknown rotor speed that maximizes the aerodynamic rotor power, $P_{\text{aero}}(t)$, for a particular wind speed, $v(t)$, and blade pitch angle, β . As stated in Remark 1.1, $P_{\text{aero}}(t)$ is unmeasurable, therefore the estimated captured power,

$\hat{P}_{\text{aero}}(t)$, is used as the cost function to be optimized. The optimum seeking algorithm selected is the Successive Quadratic Estimator (SQE). The advantage of using this algorithm over conventional methods, such as the Golden Section Search and Simplex, is that no initial cost function values or bounds on the functional values are required. The estimator approximates the unimodal cost function, $\hat{P}_{\text{aero}}(\hat{\omega}(t))$, as a quadratic function over a local bound and successively uses this property to predict the location of ω^* , the optimum rotor speed [27].

To ensure that $\omega_d(t)$, $\dot{\omega}_d(t)$ and $\ddot{\omega}_d(t)$ are bounded, a filter based form of the SQE is used, wherein at each iteration (new guess), $\omega_d[n]$ is passed through a set of third order stable and proper low pass filters to generate continuous bounded signals for $\omega_d(t)$, $\dot{\omega}_d(t)$ and $\ddot{\omega}_d(t)$. The following filters are used in this study:

$$\omega_d(t) = \frac{\zeta_1}{s^3 + \zeta_2 s^2 + \zeta_3 s + \zeta_4} \omega_d[n] \quad (62)$$

$$\dot{\omega}_d(t) = \frac{\zeta_1 s}{s^3 + \zeta_2 s^2 + \zeta_3 s + \zeta_4} \omega_d[n] \quad (63)$$

$$\ddot{\omega}_d(t) = \frac{\zeta_1 s^2}{s^3 + \zeta_2 s^2 + \zeta_3 s + \zeta_4} \omega_d[n] \quad (64)$$

where $\zeta_1, \zeta_2, \zeta_3, \zeta_4 \in \mathbb{R}^+$ are filter constants. The optimization algorithm waits until certain error thresholds are met before making the next guess (*i.e.*, if $|\omega_d(t) - \omega_d[n]| \leq \bar{e}_1$, $|\tilde{f}(\cdot)| \leq \bar{e}_2$ and $|\omega(t) - \omega_d(t)| \leq \bar{e}_3$ then $n = n+1$ where $\bar{e}_1, \bar{e}_2, \bar{e}_3 \in \mathbb{R}^+$ are threshold constants and $n \in \mathbb{Z}^+$).

VI. SIMULATION RESULTS

A numerical case study is presented in this section to demonstrate the performance of the control strategy introduced in Section 3 and the numerical-based optimum seeking reference trajectory generator in Section 5 using MATLAB/Simulink. The plant model in (5) was assumed to correspond to a small wind turbine, possessing the following system nonlinearity

$$f(\cdot) = -\frac{1}{2} \rho_a A \frac{C_p(\lambda)}{\omega} v^3 \quad (65)$$

For simulation purposes, a 350W EXTRACTOR wind turbine and a 1/2 hp two-pole induction generator were selected. The simulation parameters are listed in Appendix V. The resulting rotor speed tracking error $e(t)$ and flux tracking errors $\eta_{s_1}(t)$, $\eta_{s_2}(t)$, $\eta_{r_1}(t)$ and $\eta_{r_2}(t)$ are shown

in Figs. 2, 3, 4, 5 and 6, respectively. From these figures, it can be seen that globally uniformly bounded tracking errors have been achieved under the proposed control strategy. The voltage control inputs $V_{r_1}(t)$ and $V_{r_2}(t)$ are shown in Figs. 7 and 8, respectively. The power coefficient function, $C_p(\lambda)$, for the wind turbine, illustrated in Fig. 9a, is an example curve obtained using blade-element momentum theory [28]. It may be observed that $C_p^{\text{max}} = 0.4405$ occurs when $\lambda^* = 3.5$ which corresponds to $\omega^* = 5.296$. The actual power efficiency measure, $C_p(t)$, shown in Fig. 9b, shows that $C_p(t) \rightarrow 0.4401$ as $\omega(t) \rightarrow 5.3569$ illustrated in Fig. 10. Additionally, the copper loss, $P_{\text{loss}}(t)$, desired stator flux, $\Psi_{s_1}^d(t)$ and estimator error $\tilde{f}(t)$ are shown in Figs. 11, 12 and 13, respectively. Overall, the simulation results demonstrate that the proposed control strategy performed satisfactorily and shows a robust response to structural uncertainties.

VII. CONCLUSION

A nonlinear control strategy has been developed for a variable speed wind turbine system to optimize the energy captured by the wind turbine for a particular blade pitch angle. A desired rotor speed trajectory generator is presented that seeks the unknown optimal rotor speed while ensuring the trajectory remains bounded and sufficiently differentiable. To track the desired trajectory, a robust tracking controller is developed. The proposed controller is proven to yield a globally uniformly ultimately bounded results while keeping the closed-loop system stable via Lyapunov-based analysis. Simulation results were provided to verify the effectiveness of the control strategy. Future research will involve the implementation of the control strategy on the EXTRACTOR wind turbine and eliminating the assumption of constant or slowly time varying wind speed.

APPENDIX I—GENERATING $\Psi_{s_1}^d(t)$ ONLINE

$\Psi_{s_1}^d(t)$ is designed to be a strictly positive function that ensures $\Psi_{s_1}^d(t)$, $\dot{\Psi}_{s_1}^d(t)$, $\ddot{\Psi}_{s_1}^d(t)$ are bounded and an optimum reduction in copper loss. The copper loss denoted by $P_{\text{loss}}(t)$, is defined as

$$P_{\text{loss}} = \text{Power}_{\text{in}} - \text{Power}_{\text{out}} \quad (66)$$

$$P_{\text{loss}} = I_r^T V_r + \tau \omega - I_s^T I_s R_L$$

Substituting (16), (17), (19) and (20) into (66) results in

$$P_{\text{loss}} = (\kappa_1 \Psi_r - \kappa_2 \Psi_s)^T (\dot{\Psi}_r + R_r \kappa_1 \Psi_r - R_r \kappa_2 \Psi_s + J \Psi_r \omega_s - n_p \omega J \Psi_r) + \tau \omega - R_L (\kappa_1 \Psi_s - \kappa_2 \Psi_r)^T (\kappa_1 \Psi_s - \kappa_2 \Psi_r). \quad (67)$$

At steady state, the system is tracking where all time derivatives equal zero and $\Psi_r \rightarrow \Psi_r^d$, $\Psi_s \rightarrow \Psi_s^d$, $\tau \rightarrow \tau_d$, $\omega \rightarrow \omega_d$ results in the following

$$P_{loss} = (\kappa_1 \Psi_r^d - \kappa_2 \Psi_s^d)^T (R_r \kappa_1 \Psi_r^d - R_r \kappa_2 \Psi_s^d - n_p \omega_d J \Psi_r^d) + \tau_d \omega_d - R_L (\kappa_1 \Psi_s^d - \kappa_2 \Psi_r^d)^T (\kappa_1 \Psi_s^d - \kappa_2 \Psi_r^d) \quad (68)$$

$$\tau_d = -\hat{f}_s \quad \Psi_{r_2}^d = \frac{\hat{f}_s}{\alpha \Psi_{s_1}^d} \quad (69)$$

$$\Psi_{r_1}^d = \frac{\kappa_1}{\kappa_2} \Psi_{s_1}^d \quad \omega_s = \frac{R_o \kappa_2 \hat{f}_s}{\alpha \Psi_{s_1}^d} \quad (70)$$

After substituting (69) and (70) into (68), P_{loss} can be expressed as a function of $\Psi_{s_1}^d$ as

$$P_{loss} = \left[\frac{\kappa_1^4 R_r}{\kappa_2^2} + \kappa_2^2 R_r - 2\kappa_1^2 R_r \right] (\Psi_{s_1}^d)^2 + \left[\frac{\kappa_1^2 R_r \hat{f}_s^2}{\alpha^2} + \frac{\kappa_2^2 R_o \hat{f}_s^2}{\alpha^2} - \frac{R_L \kappa_2^2 \hat{f}_s^2}{\alpha^2} \right] \frac{1}{(\Psi_{s_1}^d)^2} - \frac{\kappa_2 n_p \omega_d \hat{f}_s}{\alpha} - \hat{f}_s \omega_d \quad (71)$$

The expression in (71) is then used as cost function in a filter-based SQE numerical minimization algorithm, similar to Section V, with $\Psi_{s_1}^d$ as the functional value. This ensures an optimum reduction in copper losses and that $\Psi_{s_1}^d(t), \dot{\Psi}_{s_1}^d(t), \ddot{\Psi}_{s_1}^d(t) \in \mathcal{L}_\infty$.

APPENDIX II—DEFINITIONS OF Ω_i AND Θ_j

The terms Ω_i and Θ_j where $i=1, \dots, 13$ and $j=1, \dots, 13$, introduced in (34) and (35), are given by

$$\begin{aligned} \Theta_1 &= \frac{\kappa_1}{\kappa_2} - \frac{(R_o \kappa_1 - \kappa_{s_1})}{R_o \kappa_2} \\ \Theta_2 &= \frac{\kappa_1 (R_o \kappa_1 - \kappa_{s_1})}{\kappa_2 R_o \kappa_2} + R_r \kappa_2 \\ \Theta_3 &= R_o \kappa_1 - \kappa_{s_1} + R_r \kappa_1 \\ \Theta_4 &= n_p \omega - \omega_s + \frac{\alpha \hat{f}_s}{R_o \kappa_2 M_m} \end{aligned}$$

$$\Theta_5 = \left[\frac{\hat{f}_s \dot{\Psi}_{s_1}^d}{R_o \kappa_2 \Psi_{s_1}^d} + \frac{\hat{f}_s}{R_o \kappa_2} \left[\frac{K}{M_m \Psi_{s_1}^d} - \frac{2\rho}{M_m \varepsilon \Psi_{s_1}^d} \frac{\partial \rho}{\partial \omega} e \right] + \frac{\rho^2}{M_m \varepsilon \Psi_{s_1}^d} \right] - \frac{\hat{f}_s}{R_o \kappa_2 \Psi_{s_1}^d} + \frac{M_m \ddot{\omega}_d}{R_o \kappa_2 \Psi_{s_1}^d} - \frac{M_m \dot{\omega}_d \dot{\Psi}_{s_1}^d}{R_o \kappa_2 \Psi_{s_1}^d} + \frac{\alpha \Psi_{r_2}^d}{R_o \kappa_2 M_m} \left[K + \frac{\rho^2}{\varepsilon} \right]$$

$$\Theta_6 = \left[\frac{K \dot{\Psi}_{s_1}^d}{\Psi_{s_1}^d} + \frac{K^2 \varepsilon + 2K \rho^2}{M_m \varepsilon \Psi_{s_1}^d} - \frac{2\rho}{\varepsilon \Psi_{s_1}^d} \frac{\partial \rho}{\partial \omega} \dot{\omega}_d + \frac{\rho^4}{\varepsilon \Psi_{s_1}^d} \right]$$

$$\Theta_7 = \frac{1}{R_o \kappa_2} \left[\frac{2K \rho}{M_m \varepsilon \Psi_{s_1}^d} \frac{\partial \rho}{\partial \omega} + \frac{2\rho^3}{M_m \varepsilon^2 \Psi_{s_1}^d} \frac{\partial \rho}{\partial \omega} \right]$$

$$\Theta_8 = \left[R_o \kappa_2 + \frac{(\alpha \Psi_{r_2}^d)^2}{R_o \kappa_2 M_m} + \frac{\kappa_1}{\kappa_2} (R_o \kappa_1 - \kappa_{s_1}) + R_r \kappa_2 \right]$$

$$\Theta_9 = \frac{\alpha}{R_o \kappa_2} \left[\frac{K}{M_m \Psi_{s_1}^d} - \frac{2\rho}{M_m \varepsilon \Psi_{s_1}^d} \frac{\partial \rho}{\partial \omega} e + \frac{\rho^2}{M_m \varepsilon \Psi_{s_1}^d} \right]$$

$$\Theta_{10} = \left[\frac{\alpha^2 \Psi_{r_1}^d \Psi_{r_2}^d}{R_o \kappa_2 M_m} + \frac{(R_o \kappa_1 - \kappa_{s_1}) \omega_s}{R_o \kappa_2} \right]$$

$$\Theta_{11} = \left[\alpha - \frac{\alpha \Psi_{r_1}^d}{R_o \kappa_2} \left[\frac{K}{M_m \Psi_{s_1}^d} - \frac{2\rho}{M_m \varepsilon \Psi_{s_1}^d} \frac{\partial \rho}{\partial \omega} e + \frac{\rho^2}{M_m \varepsilon \Psi_{s_1}^d} \right] \right]$$

$$\Theta_{12} = \frac{\alpha^2 \Psi_{r_2}^d}{R_o \kappa_2 M_m}$$

$$\Theta_{13} = \left[-(R_o \kappa_1 - \kappa_{s_1}) - R_r \kappa_1 + \kappa_{r_1} + \frac{\rho_1^2}{\varepsilon_1} \right]$$

$$\Omega_1 = \frac{\hat{f}_s}{\alpha \Psi_{s_1}^d} - \left[\frac{M_m \ddot{\omega}_d}{\alpha \Psi_{s_1}^d} - \frac{M_m \dot{\omega}_d \dot{\Psi}_{s_1}^d}{\alpha \Psi_{s_1}^d} - R_r \kappa_1 \Psi_{r_2}^d + n_p \omega \Psi_{r_1}^d - \Psi_{r_1}^d \omega_s \right]$$

$$\Omega_2 = \left[\frac{K}{\alpha M_m \Psi_{s_1}^d} - \frac{2\rho}{\alpha M_m \varepsilon \Psi_{s_1}^d} \frac{\partial \rho}{\partial \omega} e + \frac{\rho^2}{\alpha M_m \varepsilon \Psi_{s_1}^d} + \frac{\dot{\Psi}_{s_1}^d}{\alpha \Psi_{s_1}^d} \right]$$

$$\Omega_3 = \left[\alpha \Psi_{s_1}^d - \frac{K \dot{\Psi}_{s_1}^d}{\alpha \Psi_{s_1}^d} - \frac{K^2}{\alpha M_m \Psi_{s_1}^d} - \frac{2K \rho^2}{\alpha M_m \varepsilon \Psi_{s_1}^d} + \frac{2\rho}{\alpha \varepsilon \Psi_{s_1}^d} \frac{\partial \rho}{\partial \omega} \dot{\omega}_d - \frac{\rho^4}{\alpha M_m \varepsilon^2 \Psi_{s_1}^d} - \frac{\rho^2 \dot{\Psi}_{s_1}^d}{\alpha \varepsilon \Psi_{s_1}^d} \right]$$

$$\begin{aligned} \Omega_4 &= \left[\frac{K}{M_m \Psi_{s_1}^d} - \frac{\left(2\rho \frac{\partial \rho}{\partial \omega} e - \rho^2\right)}{M_m \varepsilon \Psi_{s_1}^d} \right] \\ \Omega_5 &= \left[R_r \kappa_1 - \frac{K \Psi_{s_1}^d}{M_m \Psi_{s_1}^d} + \frac{\left(2\rho \frac{\partial \rho}{\partial \omega} e - \rho^2\right) \Psi_{s_1}^d}{M_m \varepsilon \Psi_{s_1}^d} + R_r \kappa_2 \right] \\ \Omega_6 &= \frac{\alpha}{R_o \kappa_2} \left[\frac{K}{M_m} - \frac{\left(2\rho \frac{\partial \rho}{\partial \omega} e - \rho^2\right)}{M_m \varepsilon} \right] \\ \Omega_7 &= \frac{\Omega_6}{\Psi_{s_1}^d} \\ \Omega_8 &= \frac{R_o \kappa_2}{\alpha} \Omega_6 \\ \Omega_9 &= \left[\frac{K}{M_m} - \frac{\left(2\rho \frac{\partial \rho}{\partial \omega} e - \rho^2\right)}{M_m \varepsilon} - R_r \kappa_1 + \kappa_1 + \frac{\rho_2^2}{\varepsilon_2} \right] \\ \Omega_{10} &= \left[\frac{2K\rho \frac{\partial \rho}{\partial \omega}}{\alpha M_m \varepsilon \Psi_{s_1}^d} + \frac{2\rho^3 \frac{\partial \rho}{\partial \omega}}{\alpha M_m \varepsilon^2 \Psi_{s_1}^d} \right] \end{aligned}$$

where $\kappa_1, \kappa_2 \in \mathbb{R}^+$ are control gains, $\varepsilon_1, \varepsilon_2 \in \mathbb{R}^+$ are small constants and $\rho_1(\cdot), \rho_2(\cdot) \in \mathbb{R}^+$ are known functions designed in Appendix III.

APPENDIX III—DESIGN OF $\rho(\cdot)$, $\rho_1(\cdot)$ AND $\rho_2(\cdot)$

The functions $\rho(\cdot)$, $\rho_1(\cdot)$ and $\rho_2(\cdot)$ are designed to ensure that the conditions in Remarks 2.1 and 3.5 are met

$$\rho(\cdot) = \left| \frac{1}{2} \rho_a A \frac{0.45}{\omega} v^3 \right| \quad (72)$$

$$\rho_1(\cdot) = \left| \frac{\rho(\cdot)}{R_s \kappa_2 M_m \Psi_{s_1}^d} \left[\frac{2\rho |\partial \rho| e^2 + 2\rho^2 |e|}{\varepsilon} + \frac{2\rho^2 |e|}{\varepsilon} + 2K |e| + M_m |\dot{\omega}_d| + |\hat{f}_s| \right] \right| \quad (73)$$

$$\rho_2 = \left| \frac{\rho(\cdot)}{\alpha M_m \Psi_{s_1}^d} \left(K + \frac{\rho(\cdot) + 2\rho |\partial \rho e|}{\varepsilon} \right) \right|. \quad (74)$$

APPENDIX IV—PROOF OF LEMMA

The equation (50) can be substituted into (53) and then integrated in time to obtain

$$\begin{aligned} \int_{t_0}^t L(v) dv &= \int_{t_0}^t k \tilde{\omega}(v) \left(\dot{f}(v) - \rho_0 \operatorname{sgn}(\tilde{\omega}(v)) \right) dv \\ &+ \left[\int_{t_0}^t \dot{\tilde{\omega}}(v) \dot{f}(v) d\tau \right] \\ &- \rho_0 \int_{t_0}^t \dot{\tilde{\omega}}(v) \operatorname{sgn}(\tilde{\omega}(v)) d\tau. \end{aligned} \quad (75)$$

The bracketed term in (75) may be integrated by parts to obtain the following expression

$$\begin{aligned} \int_{t_0}^t L(v) dv &= \int_{t_0}^t k \tilde{\omega}(v) \left(\dot{f}(v) - \frac{\ddot{f}(v)}{k} \right. \\ &- \rho_0 \operatorname{sgn}(\tilde{\omega}(v)) \left. \right) dv \\ &+ \tilde{\omega}(t) \dot{f}(t) - \tilde{\omega}(t_0) \dot{f}(t_0) \\ &- \rho_0 \left| \tilde{\omega}(t) \right| + \rho_0 \left| \tilde{\omega}(t_0) \right|. \end{aligned} \quad (76)$$

An upper bound on the right hand side of (76) can be written as

$$\begin{aligned} \int_{t_0}^t L(v) dv &\leq \int_{t_0}^t k \left| \tilde{\omega}(v) \right| \left(\left| \dot{f}(v) \right| + \frac{\left| \ddot{f}(v) \right|}{k} - \rho_0 \right) dv \\ &+ \rho_0 \left| \tilde{\omega}(t_0) \right| - \tilde{\omega}(t_0) f(t_0) \\ &+ \left| \tilde{\omega}(t) \right| \left(\left| \dot{f}(t) \right| - \rho_0 \right) \end{aligned} \quad (77)$$

From (77), it is clear that if $\rho_0 > \left| \dot{f}(\cdot) \right| + \frac{\left| \ddot{f}(\cdot) \right|}{k}$, then the Lemma holds.

APPENDIX V—SIMULATION PARAMETERS

Table I lists the parameter values used in the numerical simulation of Section VI.

TABLE I. SIMULATION PARAMETERS AND VALUES

Parameters	Value	Units
K	50	-
k_f	10	-
L_s	0.078	H
M	0.571	H
M_m	2.4	kg.m ²
n_p	1	-
R	1.52	m
R_L	1	Ω

R_r	7.25	Ω
R_s	5.55	Ω
v	2.3	m/s ²
β	2.4	deg
Δ	10	-
ε	100	-
ε_1	1	-
ε_2	1	-
κ_{r_1}	1	-
κ_{r_2}	1	-
κ_{s_1}	50	-
κ_{s_2}	50	-
ρ_a	1.2	kg/m ³
σ	0.25	-

REFERENCES

[1] K. Johnson, L. Fingersh, M. Balas, and L. Pao, "Methods for increasing region 2 power capture on a variable-speed wind turbine", *J. Solar Energy Eng.*, vol. 126, no. 4, pp. 1092-1100, 2004.

[2] U. Ozbay, E. Zengeroglu and S. Sivrioglu, "Adaptive backstepping control of variable speed wind turbines," *International Journal of Control*, vol. 81, no. 6, pp. 910-919, Jun. 2008.

[3] Y. Song, B. Dhinakaran, and X. Bao, "Variable speed control of wind turbines using nonlinear and adaptive algorithms," *J. Wind Eng. Ind. Aerodyn.*, vol. 85, no. 3, pp. 293-308, Apr. 2000.

[4] M. Hand and M. Balas, "Non-linear and linear model based controller design for variable-speed wind turbines," pp. 1-8. NREL Report No. CP-500-26244.

[5] B. Liebst, "Pitch control system for large-scale wind turbines," *J. of Energy*, vol. 7, no. 2, pp. 182-192, 1983

[6] T. Knudsen, P. Andersen, and S. Tiffner-Clausen, "Comparing PI and robust control pitch controllers on a 400KW wind turbine by full scale tests," Department of Control Engineering, Aalborg University, Aalborg, Denmark, Tech. Rep. R-97-4174, 1997.

[7] K. Stol and M. Balas, "Full-state feedback control of a variable-speed wind turbine: A comparison of periodic and constant Gains", *J. of Solar Energy Eng.*, vol. 123, no. 4, pp. 319-326, 2001.

[8] E. Iyasere, M. Salah, D. Dawson and J. Wagner, "Nonlinear robust control to maximize energy capture in a variable speed wind turbine", *Proc. of the American Control Conference*, pp. 1824-1829, Seattle, WA, Jun. 2008.

[9] R. Chedid, S. Karaki, and C. El-Chamali, "Adaptive fuzzy control for wind-diesel weak power systems," *IEEE Trans. Energy Conversion*, vol. 15, no. 1, pp. 71-78, Mar. 2000.

[10] X. Zhang, W. Wang and Y. Liu, "Fuzzy control of variable speed wind turbine," *Proc. 6th World Congress on Intelligent Control and Automation*, pp. 3872-3876, Dalian, China, 2006.

[11] T. Thiringer and J. Luomi, "Comparison of reduced-order dynamic models of induction machines," *IEEE Trans. Power Syst.*, vol. 16, no. 1, pp. 119-126, Feb. 2001.

[12] A. Tapia, G. Tapia, J. Ostolaza, and J. Saenz, "Modeling and control of a wind turbine driven doubly fed induction generator," *IEEE Trans. Energy Conversion*, vol. 18, no. 2, pp. 194-204, Jun. 2003.

[13] A. Mullane and M. O'Malley, "Inertial response of induction-machine-based wind turbines" *IEEE Trans. Power Syst.*, vol. 20, no. 3, pp. 1496-1503, Aug. 2005.

[14] J. Cathey, R. Calvin, and A. Ayoub, "Transient load model of an induction motor," *IEEE Trans. Power Apparatus and Syst.*, vol. 92, no. 4, pp. 1399-1406, Jul. 1973.

[15] S. Muller and M Deicke "Doubly fed induction generator systems for wind turbines," *IEEE Ind. Appl. Mag.*, pp 26-33, Jun. 2002.

[16] J. Hu and D. Dawson "Adaptive control of induction motor systems despite rotor resistance uncertainty," *Automatica*, vol. 32, no. 8, pp. 1127-1143, 1996.

[17] R. Datta and V. Ranganathan, "A simple position-sensorless algorithm for rotor-side field-oriented-control of wound rotor induction machine," *IEEE. Trans. Ind. Elect.*, vol. 48, no. 4, pp. 786-793, Aug. 2001.

[18] R. Pena, J. Clare, and G. Asher, "Doubly fed induction generator using back to back PWM converters and its application to variable-speed wind-energy generation," *IEE Proc. Electr. Power Appl.*, vol. 143, no. 3, pp. 231-241, May 1996.

[19] R. Marino, S. Peresada, and P. Valigi, "Adaptive input-output linearizing control of induction motors," *IEEE Trans. Automat. Contr.*, vol. 38, no. 2, pp. 208-221, Feb. 1993.

[20] R. Marino, S. Peresada and P. Tomei, "Global adaptive output feedback control of induction motors with uncertain rotor resistance," *IEEE Trans. Automat. Contr.*, vol. 44, pp. 967-983, May 1999.

[21] K. Gopakumar, V. Ranganathan, and S. Bhat, "Vector control of induction motor with split phase stator windings," *Conf. Rec. IEEE-IAS Annu. Meeting, Denver, CO.*, pp. 569-574, Oct. 1994.

[22] R. Datta and V. Ranganathan, "Variable-speed wind power generation using doubly fed wound rotor induction machine—a comparison with alternative schemes," *IEEE Trans. Energy Conv.*, vol. 17, no. 3, pp. 414-421, Sept. 2002.

[23] R. Datta and V. Ranganathan, "Direct Power control of grid-connected wound rotor induction machine without rotor position sensors," *IEEE Trans. Power Elec.*, vol. 16, no. 3, pp. 390-399, May 2001.

[24] P. Krause, *Analysis of Electrical Machinery*. New York: McGraw Hill, 1986.

[25] P. Kokotovic, "The joy of feedback: nonlinear and adaptive," *IEEE Control Syst. Mag.*, vol. 12, no. 3, pp. 7-17, Jun. 1992.

[26] J. Slotine and W. Li, *Applied Nonlinear Control*, Englewood Cliffs, NJ: Prentice Hall, 1991.

[27] G. Reklaitis, A. Ravindran, and K. Ragsdell, *Engineering Optimization*, Hoboken, NJ: John Wiley & Sons, 1983, pp. 41-130.

[28] NWTC Design Codes (WT_Perf by Marshall Buhl), <http://wind.nrel.gov/designcodes/simulators/wtperf/>, Aug. 1, 2007.

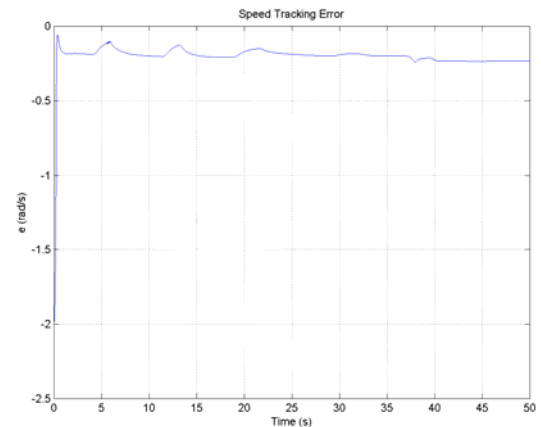


Figure 2. Rotor speed tracking error $e(t)$

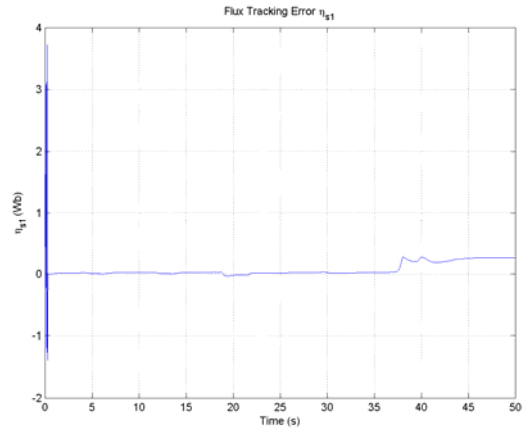


Figure 3. Stator flux tracking error $\eta_{s1}(t)$

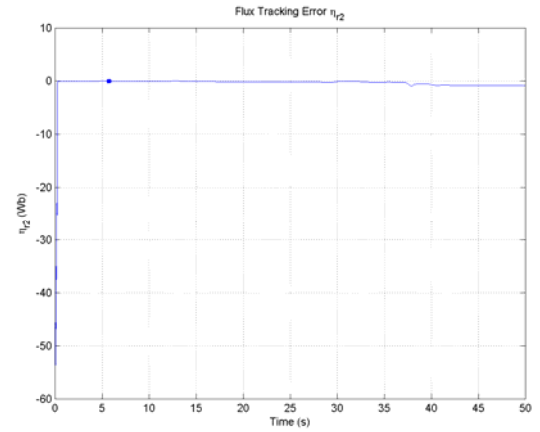


Figure 6. Rotor flux tracking error $\eta_{r2}(t)$

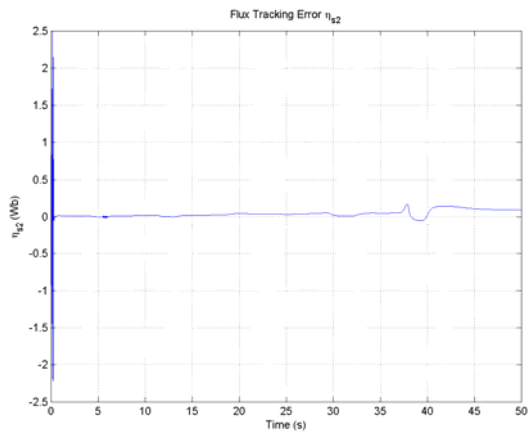


Figure 4. Stator flux tracking error $\eta_{s2}(t)$

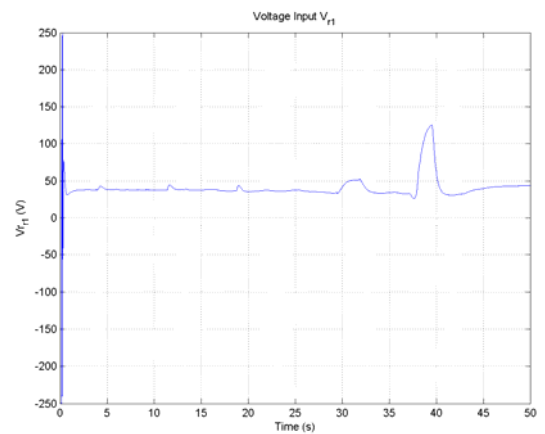


Figure 7. Voltage control input $V_{r1}(t)$

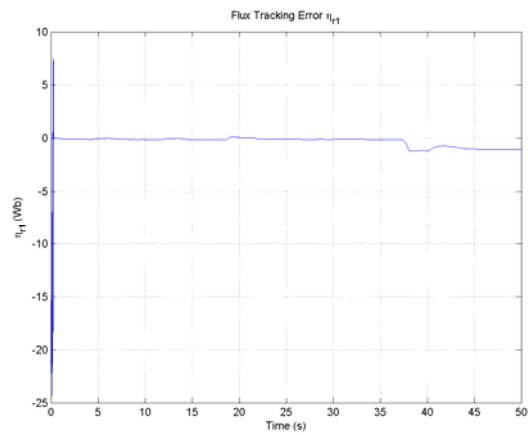


Figure 5. Rotor flux tracking error $\eta_{r1}(t)$

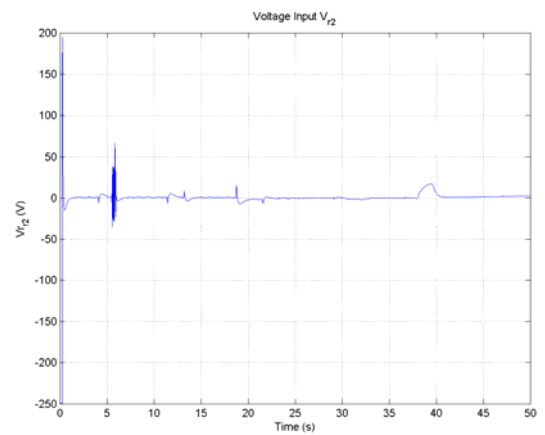


Figure 8. Voltage control input $V_{r2}(t)$

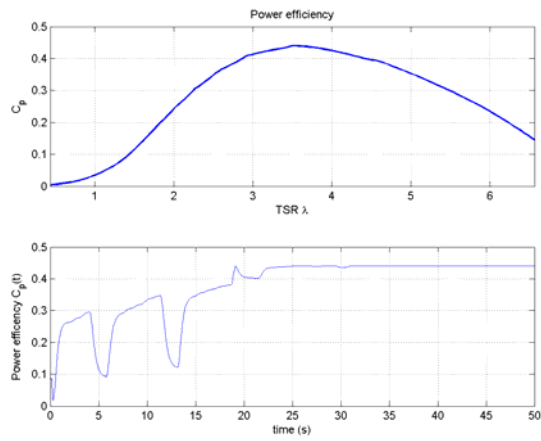


Figure 9. (a) Power efficiency curve of the simulated wind turbine, and (b) Rotor power coefficient $C_p(t)$ resulting from optimization algorithm

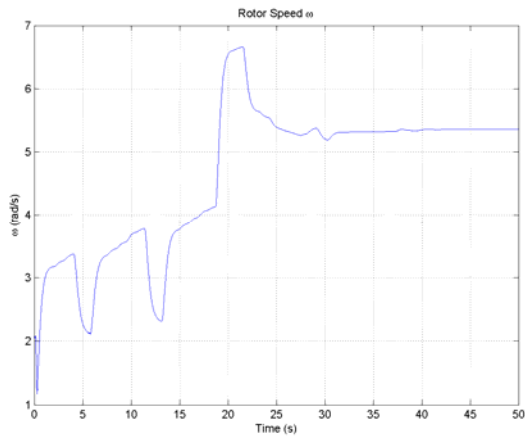


Figure 10. Rotor Speed $\omega(t)$

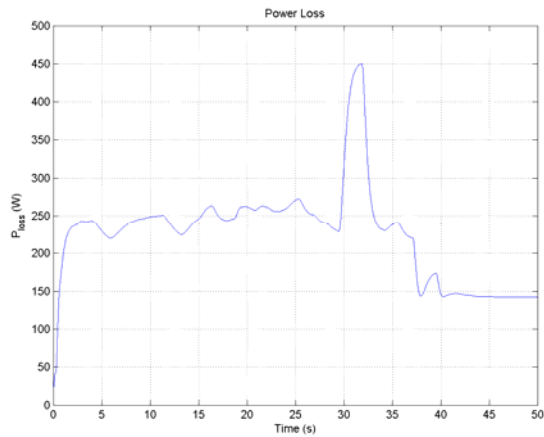


Figure 11. Copper losses $P_{loss}(t)$

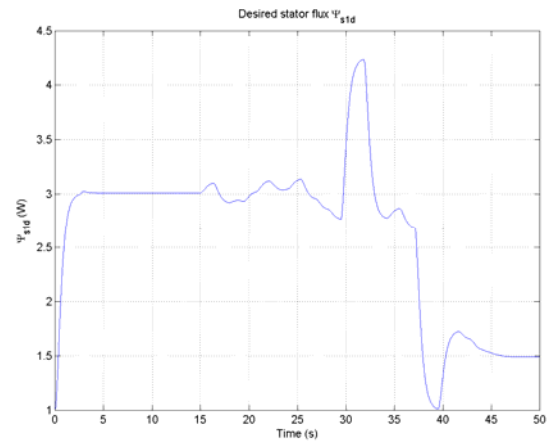


Figure 12. Desired Stator flux $\Psi_{s_1}^d(t)$

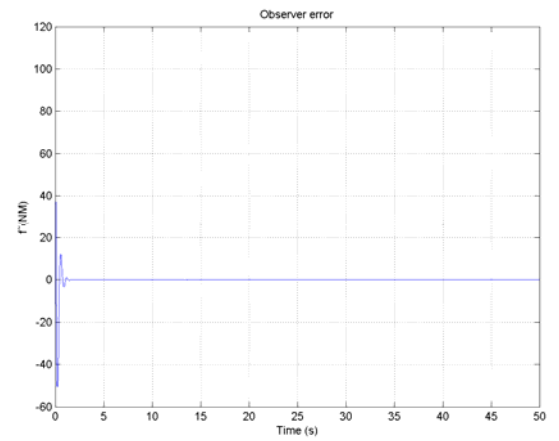


Figure 13. Nonlinearity observation error $\tilde{f}(t)$